




Nano-Powdered Calcium Carbonate Reference Materials: Significant Progress for Microanalysis?

Klaus Peter Jochum (1)* , Dieter Garbe-Schönberg (2), Marina Veter (1, 3), Brigitte Stoll (1), Ulrike Weis (1) , Michael Weber (1, 4) , Federico Lugli (5), Anna Jentzen (1), Ralf Schiebel (1), Jasper A. Wassenburg (1), Dorrit E. Jacob (3) and Gerald H. Haug (1, 6)

(1) Climate Geochemistry Department, Max Planck Institute for Chemistry, P.O. Box 3060, 55020, Mainz, Germany

(2) Institute of Geosciences, Kiel University, Ludewig-Meyn-Straße 10, 24118, Kiel, Germany

(3) Department of Earth and Planetary Sciences, Macquarie University, 12 Wallys Walk, 2109, Sydney, NSW, Australia

(4) Institute of Geosciences, Johannes Gutenberg University, J.-J. Becher-Weg 21, 55128, Mainz, Germany

(5) Department of Cultural Heritage, University of Bologna, 48121, Ravenna, Italy

(6) ETH Zürich, Sonneggstrasse 5, 8092, Zürich, Switzerland

*Corresponding author. e-mail: k.jochum@mpic.de

Homogeneity, mass fractions of about forty trace elements and Sr isotope composition of Ca carbonate reference materials (RMs) between original and nano-powdered pellets are compared. Our results using nanosecond and femtosecond LA-(MC)-ICP-MS show that the nano-pellets of the RMs MACS-3NP, JCp-1NP and JcT-1NP are about a factor of 2–3 more homogeneous than the original samples MACS-3, JCp-1 and JcT-1, and are therefore much more suitable for microanalytical purposes. With the exception of Si, the mass fractions of the synthetic RM MACS-3 agree with its fine-grained analogue MACS-3NP. Very small, but significant, differences between original and nano-pellets are observed in the RMs JCp-1 and JcT-1 for some trace elements with very low contents, indicating the need for re-certification. Strontium mass fractions in the analysed RMs are high (1500–7000 mg kg⁻¹), and their isotope compositions determined by LA-MC-ICP-MS in the original and the nano-pellets agree within uncertainty limits.

Keywords: laser ablation-inductively coupled plasma-mass spectrometry, microanalysis, reference materials, carbonate, homogeneity.

Received 28 Feb 19 – Accepted 22 Jul 19

Geological and biological materials play an increasing role as palaeoclimate archives with incremental layers of systematically changing compositions reflecting environmental conditions during their formation (e.g., Yang *et al.* 2014, Wassenburg *et al.* 2016a, Fehrenbacher *et al.* 2017). Many of them, such as speleothems, foraminifers, ostracods, corals and mussels, have a calcareous matrix. Some of them are very small in the 10–100 µm range and/or have closely spaced compositionally different layers. Laser ablation-inductively coupled plasma-mass spectrometry (LA-ICP-MS) has become a suitable technique for microanalysis of these materials (e.g., Wassenburg *et al.* 2016b, Jochum *et al.* 2019, Jentzen *et al.* 2018, Leduc *et al.* 2014, Yang *et al.* 2014, Mertz-Kraus *et al.* 2009, Hathorne *et al.* 2009, Vetter *et al.* 2013, Caragnano *et al.* 2014, Schiebel and Hemleben 2017, Weber *et al.* 2018a), but well-characterised homogeneous reference

materials (RMs) for calibration at the nanometre to micrometre scale are needed. For such purposes, different kinds of RMs were used, for example, the silicate glasses from the National Institute of Standards and Technology (NIST), geological glasses from the United States Geological Survey (USGS), the Max Planck Institute for Chemistry (MPI-DING) and synthetic or natural carbonates (USGS) (Jochum and Enzweiler 2014). The silicate reference glasses have the advantage to be homogeneous in the nanometre to micrometre range for many elements. Some of them have high mass fractions of about 400–500 mg kg⁻¹ (e.g., NIST SRM 610, GSE-1G) and are well characterised and even certified (Jochum *et al.* 2005, 2006, 2011). One of the most important drawbacks is that the silicate matrix is quite different from that of a calcium carbonate sample. This can lead to matrix-related erroneous results in particular for volatile elements when using laser

doi: 10.1111/ggr.12292

© 2019 The Authors. *Geostandards and Geoanalytical Research* published by John Wiley & Sons Ltd on behalf of International Association of Geoanalysts

This is an open access article under the terms of the Creative Commons Attribution-NonCommercial-NoDerivs License, which permits use and distribution in any medium, provided the original work is properly cited, the use is non-commercial and no modifications or adaptations are made.

ablation systems with nanosecond (ns) pulse lengths. There is some evidence that femtosecond (fs) laser ablation reduces elemental fractionation and the inherent risk of matrix effects, in particular for silicates, carbonates and phosphates (Jochum *et al.* 2014, Ohata *et al.* 2014). To avoid matrix-dependent calibration effects for all LA-ICP-MS instruments, carbonate RMs would therefore be preferable. So far, only pressed powder pellets from synthetic or natural calcium carbonate RMs are available, such as MACS-1 or MACS-3 from the USGS (e.g., Mertz-Kraus *et al.* 2009, Jochum *et al.* 2012, Wassenburg *et al.* 2016a, Marali *et al.* 2017). The ablation of such pellets is not as reproducible as for glass samples, because the powders of the RMs are mostly coarse-grained with grain sizes of about 10–15 μm .

Tabersky *et al.* (2014) described a flame spray technique, which allows the production of synthetic materials with nano-scale grain size. Recently, Weber *et al.* (2019) used this technique to produce a carbonate RM. Garbe-Schönberg and Mueller (2014) have developed a technique to produce fine-grained nano-pellets from original carbonate powders, with grain sizes reaching into the range of nanoparticles (Figure S1).

The aim of this study is (a) to investigate the homogeneity of the original powder pellets and the corresponding nano-pellets of the synthetic RM MACS-3 and the natural carbonate RMs JCp-1 and JCT-1 by using femtosecond and nanosecond LA-ICP-MS, (b) to study possible contamination of the nano-pellets introduced during the preparation procedure, (c) to present new analytical trace element and Sr isotope data and (d) to derive reference values for the MACS-3 RM by using the new analytical data of this work, USGS compilations and already published values.

Analytical set-up

Samples

The currently available pressed powder pellet of MACS-3 as delivered by the USGS was used in this study. A new fine-grained MACS-3NP nano-pellet was investigated in comparison, which originates from the original MACS-3 powder distributed by the USGS, and was prepared at the University of Kiel by Garbe-Schönberg and Mueller (2014) using the new technique.

In addition, two natural calcium carbonate RMs of low trace element mass fractions, from the Geological Survey of Japan (GSJ) were analysed, namely JCp-1, a recent *Porites* sp. coral from Ishigaki Island (Okai *et al.* 2002), and JCT-1, a giant clam *Tridachna gigas* from Kume Island (Inoue *et al.*

2004). From both powdered samples, pressed pellets (13 mm in diameter) were made at the University of Mainz using a vacuum hydraulic press from Perkin Elmer (5 tons). Nano-pellets of these GSJ samples were also prepared at the University of Kiel by re-milling the original powders. We also investigated the original USGS pellet of MACS-1.

Analytical techniques

Trace element measurement was carried out with an Element2 sector field ICP mass spectrometer at the Max Planck Institute for Chemistry (MPIC) in Mainz. Strontium isotopes were measured with a Nu Plasma multi-collector ICP-MS instrument (first generation) at MPIC. Important operating parameters for the analysis are listed in Table 1. Tuning was conducted with NIST SRM 612 to minimise oxide production (for both ns and fs ablation ThO/Th was < 0.3%) and elemental fractionation (in particular for fs ablation Th/U was about 1). Ca²⁺/Ca⁺ ratio in carbonates (Fietzke and Frische 2016, Jochum *et al.* 2019) was uniform and independent from laser parameters. For each sample, nine line scan analyses (length 300 μm ; scan speed = 5 $\mu\text{m s}^{-1}$) were performed. Two different laser ablation systems with different operating conditions (Jochum *et al.* 2014) were used:

- (1) a NWR Femto laser ablation system with 130 femtosecond pulse length and 200 nm wavelength. Two different spot sizes (25 μm , 55 μm) were taken to investigate specimen homogeneity. For all trace element analyses, the pulse repetition rate (PRR) was 50 Hz and the fluence was 0.5–0.7 J cm⁻². Mg/Ca measurements using the recently developed single pulse technique (Jochum *et al.* 2019) were performed with a spot size of 55 μm , a PRR of 1 Hz at a fluence of < 0.5 J cm⁻².
- (2) a UP213 Nd:YAG laser with a pulse length of 5 ns and 213 nm wavelength. With this laser ablation system, 25 μm and 55 μm spot size for line scans at a PRR of 10 Hz were employed. The fluence was approximately 10 J cm⁻².

Both systems are equipped with the ESI high-performance large format cell. The washout time is about 1 s at ca. 95% level. Altogether, the mass fractions of forty trace elements were determined (Tables 2a–e, Figure 1) using ⁴³Ca as internal standard and NIST SRM 610 for calibration of the measurements. Data reduction followed a programmed Microsoft Excel routine (Jochum *et al.* 2007). Calcium mass fractions of the carbonates are taken from publications (GeoReM database). The relative sensitivity factors were determined for fs- and ns-laser ablation.

Table 1.
Operating parameters for the ICP-MS and laser ablation systems used

ICP-MS			Laser ablation system			
Operating parameter	Element2	Nu Plasma	Operating parameter	UP 213 trace elem.	UP 213 Sr isotopes	NWR Femto trace elem.
rf power (W)	1150	1350	Wavelength (nm)	213	213	200
Cooling gas (Ar) flow rate (l min ⁻¹)	16	13	Pulse length (ns)	5	5	< 0.00013
Auxiliary gas (Ar) flow rate (l min ⁻¹)	1	0.93	Fluence (J cm ⁻²)	9–11	10–15	0.5–0.7
Sample gas (Ar) flow rate (l min ⁻¹)	0.6	0.7	Spot size (μm)	25, 55	55–80	25, 55
Carrier gas (He) flow rate (l min ⁻¹)	0.7	0.7	Pulse repetition rate (Hz)	10	10	50
Sample time (s) (= dwell time per <i>m/z</i>)	0.002	0.2	Warm up (s)	10	45	20
Detector mode	Counting analogue	Faraday collectors	Ablation time (s)	100–200	150	25–60
Mass resolution	300	300	Wash out (s)	30	30	30
			Scan speed (μm s ⁻¹)	5	5	5

Isotopes used for analysis are listed in Table 2a. The whole measuring time for one run (forty elements) was 1.3 s. The range of limits of detection (LODs) defined as 3 × standard deviation of the blank are listed in Tables 2a and b. For ns ablation using a fluence of 10 J cm⁻² LODs varied between about 300 and 0.0001 mg kg⁻¹ for the different elements. LODs are a factor of about 4 higher when using femtosecond ablation, mainly because of its gentle ablation using low fluence.

High-depth-resolution single-shot Mg/Ca measurements were only performed with the fs laser (Jochum *et al.* 2019, Figure 2). To generate 2D mapping of both the original pellets and nano-pellets of MACS-3 and JCI-1, line scan analyses were performed with the UP213 laser system with a spot size of 100 μm, spacing of 100 μm and a scan speed of 30 μm s⁻¹ (Figure 3). NIST SRM 612 was used for calibration with ⁴³Ca as internal standard and applying the Jochum *et al.* (2011) reference values. All calculations for trace element mass fraction are performed by the MapIT software, following the protocol presented by Sfoma and Lugli (2017).

In addition, *in situ* Sr isotope ratio measurements were performed using LA-MC-ICP-MS, following the protocol of Weber *et al.* (2017, 2018b). A Nu Plasma (first generation) MC-ICP-MS was coupled to a New Wave UP213 Nd:YAG laser ablation system at MPIC. Prior to analyses, peak shape and coincidence were optimised using the NIST SRM 987 solution while coupling the instrument to a CETAC Aridus II desolvating nebuliser system. For the laser ablation measurements, line scans of 750 μm length with a

scan speed of 5 μm s⁻¹, a spot size of 55–80 μm and an energy output of 50–70% (depending on the Sr concentration and the ablation behaviour of the RM) were applied, resulting in a fluence of 5.5–18 J cm⁻². Pre-ablation was performed prior to each analysis to remove surface contamination. Background signals (including Kr) were corrected by subtracting the on-peak baseline obtained during 45 s background acquisition with laser off. Potential interferences of double charged REEs were corrected by monitoring ¹⁷¹Yb²⁺ and ¹⁶⁷Er²⁺. Molecular interferences were found to be negligible due to usual intensities < 0.2 mV for *m/z* = 82. Mass bias correction was performed using the exponential law and corrected for ⁸⁶Sr/⁸⁸Sr of 0.1194. The intensity of ⁸⁵Rb was monitored and used to correct for ⁸⁷Rb at mass 87 by calculating the fraction of ⁸⁷Rb using a constant ⁸⁷Rb/⁸⁵Rb of 0.3857. For Rb, we assumed the same instrumental mass bias observed for Sr.

Results and discussion

Homogeneity

Homogeneity is a fundamental requirement for each RM. For microanalytical RMs, homogeneity should be ensured for test portion masses of less than 1 μg (Jochum and Enzweiler 2014). We tested the homogeneity of the pellets from the original RMs and the nano-pellets with different procedures:

- (1) evaluation of the repeatability (RSD) of nine independent line scan measurements of 300 μm length

Table 2a.
Mass fractions (mg kg^{-1}) and standard deviations ($1s$) of MACS-3 and MACS-3NP (nano-pellet) samples using femtosecond laser ablation with different spot sizes

Spot size	Isotope used	MACS-3						MACS-3NP				LOD (range) mg kg^{-1}
		55 μm	55 μm	25 μm	25 μm	Mean MACS-3		55 μm	25 μm	Mean MACS-3NP		
		mg kg^{-1}	mg kg^{-1}	mg kg^{-1}	mg kg^{-1}	mg kg^{-1}	$1s$	mg kg^{-1}	mg kg^{-1}	mg kg^{-1}	$1s$	
Li	7	63	67.3	67.2	65.8	65.8	2.0	58.1	67.4	62.8	6.6	0.7–1
B	11	7.91	8.22			8.07	0.22	7.64	8.80	8.22	0.82	0.7–1
Na	23	5920	6100	6500	6700	6310	360	5560	6440	6000	620	100–200
Mg	25	1550	1700		1670	1640	80.0	1540.0	1430.00	1490	80	1.5–3
Al	27	361	361	367	393	370	16	386	415	400	21	3–10
Si	29	(240)	(280)			(260)		4020	3940	3980	57	300–500
P	31	88.5	120	80.5	124	103	22	102	122	112	14	50–80
Ti	47	43.6	47.7		51.5	47.6	3.9	48.8	24.8	37	17	4–10
V	51	42.9	43.6	41.4	46.6	43.6	2.2	47.7	45.7	46.7	1.4	0.1–0.3
Cr	53	105	106	110	126	112	10	114	114	114	0.3	1–3
Mn	55	506	512	501	532	513	14	512	498	505	10	2–5
Fe	57	8830	10200		10700	9910	970	9580	8050	8820	1080	50–150
Co	59	54.0	57.8	55.9	56.7	56.1	1.6	55.1	57.3	56.2	1.6	0.3–0.8
Ni	60	53.8	57.1	57.2	59.6	56.9	2.4	56.2	61.1	58.7	3.5	3–6
Cu	63	112	122	119	124	119	5	114	121	118	5	0.6–1
Zn	67	138	178	140	161	154	19	151	179	165	19	3–10
Rb	85	(0.064)		(0.1)		(0.082)		(0.044)		(0.044)		0.06–0.1
Sr	86	6730	6870	6820	6920	6840	80	7090	6840	6970	180	4–10
Y	89	22.5	23.6	21.3	22.5	22.5	1.0	23.4	22.6	23.0	0.6	0.003–0.01
Zr	90	7.92	8.51	7.97	9.12	8.38	0.56	8.91	8.85	8.88	0.05	0.005–0.01
Cs	133	0.018	(0.008)			(0.01)		(0.008)		(0.008)		0.01–0.03
Ba	137	57.4	60.5	55.5	62.6	59.0	3.2	60.1	59.2	59.7	0.6	0.3–0.5
La	139	10.8	11.5	10.0	11.1	10.9	0.6	11.4	10.7	11.1	0.5	0.005–0.01
Ce	140	11.1	11.8	10.4	11.8	11.3	0.7	11.7	11.1	11.4	0.4	0.002–0.007
Pr	141	11.8	12.3	11.0	11.7	11.7	0.5	12.2	11.5	11.9	0.5	0.003–0.007
Nd	143	11.1	11.4	10.9	10.4	11.0	0.4	11.6	10.9	11.2	0.5	0.02–0.06
Sm	147	10.9	11.2	10.2	11.6	11.0	0.6	11.4	10.5	11.0	0.6	0.02–0.04
Eu	151	11.5	11.8	10.7	11.4	11.4	0.5	12.0	11.3	11.6	0.5	0.02–0.04
Gd	157	10.4	10.6	9.62	10.7	10.3	0.5	10.9	10.3	10.6	0.4	0.05–0.1
Tb	159	10.4	10.5	9.57	10.3	10.2	0.4	10.8	10.1	10.5	0.5	0.003–0.01
Dy	161	10.6	10.8	10.2	10.6	10.5	0.2	11.1	10.8	11.0	0.2	0.01–0.02
Ho	165	10.9	11.0	10.1	10.9	10.7	0.4	11.4	10.8	11.1	0.4	0.002–0.004
Er	167	10.9	11.1	11.0	10.8	11.0	0.1	11.5	11.2	11.3	0.2	0.02–0.05
Tm	169	11.3	11.4	10.9	11.1	11.2	0.2	11.8	11.4	11.6	0.3	0.003–0.007
Yb	173	11.2	11.3	10.7	10.8	11.0	0.3	11.8	11.4	11.6	0.3	0.01–0.03
Lu	175	10.6	11.0	10.2	10.7	10.6	0.3	11.2	11.0	11.1	0.2	0.003–0.007
Hf	177	4.33	4.50	4.46	4.96	4.56	0.27	4.96	4.92	4.94	0.03	0.02–0.06
Pb	208	53.5	58.4	58.7	60.4	57.7	2.9	59.3	68.2	63.7	6.3	0.02–0.06
Th	232	54.7	56.8	54.4	54.8	55.2	1.1	57.7	55.8	56.7	1.3	0.0005–0.001
U	238	1.23	1.27	1.45	1.22	1.29	0.11	1.57	1.60	1.58	0.02	0.0005–0.001

LOD (range), range of limits of detection for femtosecond LA measurements, (–), mass fraction uncertain, near LOD.

performed with fs- and ns-LA using small spot sizes (25–55 μm) and low fluences. The RSD values were calculated as the variation between the nine line scans (see Table 1). Because of the low ablation depth of approximately 1–5 μm , the ablated material for one line is $< 0.5 \mu\text{g}$. RSD values obtained for nano-pellet analyses are similar as those obtained for homogeneous microanalytical reference materials (e.g., NIST SRM 61x glasses; Jochum *et al.* 2011). The

analytical repeatability for each element indicates that the chemical inhomogeneity is similar to the analytical uncertainty and hence not detectable. This is shown in Figure 1, where the RSD values of different element measurements of MACS-3, JcT-1 and JcP-1 with various mass fractions using ns ablation are plotted (see also Table S1). RSD values strongly depend on the mass fraction. The results for the nano-pellet measurements vary between about 2% (at

Table 2b.
Mass fractions (mg kg^{-1}) and standard deviations (1 s) of MACS-3 and MACS-3NP (nano-pellet) samples using 213 nm Nd:YAG laser ablation with different spot sizes

Spot size	MACS-3								MACS-3NP					LOD (range) mg kg^{-1}
	55 μm	55 μm	55 μm	25 μm	25 μm	25 μm	Mean MACS-3		55 μm	25 μm	55 μm	Mean MACS-3NP		
	mg kg^{-1}	mg kg^{-1}	mg kg^{-1}	mg kg^{-1}	mg kg^{-1}	mg kg^{-1}	mg kg^{-1}	1 s	mg kg^{-1}	mg kg^{-1}	mg kg^{-1}	mg kg^{-1}	1 s	
Li	60.6	58.0	57.2	71.4	70.3	59.3	62.8	6.4	50.4	63.5	57.1	57.0	6.6	0.4–0.8
B	9.15	9.32	7.88	8.27	12.5	7.70	9.14	1.78	6.97	9.16	5.88	7.34	1.67	0.2–0.7
Na	5500	5360	5210	6510	7300	5880	5960	800	4630	5890	5030	5180	640	30–100
Mg	1530	1450	1610	1580	1860	1620	1610	140	1480	1660	1760	1630	140	0.4–1.2
Al	362	394	379	389	358	368	375	15	345	379	346	357	19	1–3
Si	401	603	353	373			433	115	3650	4220	4510	4130	440	150–300
P	129	120	102	108		97.9	111	13	93.3	113	109	105	10	8–50
Ti	47.7	47.4	45.1	47.9		69.8	46.6	50.8	38.6	47.3	44.6	43.5	4.4	1–5
V	48.1	48.5	42.5	43.9		45.4	43.8	45.4	36.9	46.7	44.0	42.6	5.1	0.01–0.05
Cr	125	124	104	122		109	111	116	94.6	113	116	108	12	0.3–2
Mn	510	481	476	515		532	513	505	452	512	551	505	50	0.3–2
Fe	11500	11600	9720	10600		10700	10400	10800	8930	10900	16000	11900	3600	10–70
Co	54.3	50.9	51.4	54.9		62.9	56.1	55.1	48.1	56.5	58.5	54.4	5.5	0.1–0.4
Ni	57.4	55.8	52.0	55.1		56.5	56.8	55.6	48.5	56.9	59.7	55.0	5.8	0.3–2
Cu	112	105	107	117		121	117	113	98.6	113	108	106	7	0.1–0.5
Zn	121	107	106	135		138	125	122	97.1	118	168	128	37	2–7
Rb		(0.02)						(0.02)	0.030	0.054	0.033	0.039	0.013	0.01–0.07
Sr	6380	6400	6250	7080		6940	6290	6560	6140	6740	6980	6620	430	2–5
Y	19.1	18.3	18.6	23.0		20.3	20.9	20.0	18.8	21.9	19.0	19.9	1.8	0.001–0.005
Zr	8.33	8.71	8.62	8.43		6.96	7.98	8.17	7.30	8.58	7.58	7.82	0.67	0.001–0.007
Cs	0.012	0.019	0.010					0.013	0.005	(0.007)		0.012	0.012	0.005–0.02
Ba	61.9	58.5	56.9	58.4		61.6	58.7	59.3	51.1	60.7	63.9	58.6	6.7	0.05–0.2
La	10.5	9.66	10.8	10.9		10.5	10.2	10.4	9.22	11.4	11.3	10.7	1.2	0.002–0.005
Ce	10.9	9.88	10.5	11.1		11.5	10.7	10.8	9.43	11.9	12.9	11.4	1.80	0.001–0.005
Pr	11.1	10.1	11.5	12.0		11.7	11.9	11.4	9.86	12.3	13.2	11.8	1.71	0.0005–0.002
Nd	9.98	9.68	10.2	11.0		10.8	10.2	10.3	9.34	11.7	10.9	10.7	1.2	0.005–0.02
Sm	9.69	9.17	9.69	10.6		10.5	10.4	10.0	9.04	10.9	10.4	10.1	1.0	0.005–0.02
Eu	11.0	10.3	11.0	11.4		11.2	11.4	11.0	10.0	11.7	11.5	11.1	0.9	0.001–0.005
Gd	8.91	8.50	8.87	10.0		9.40	9.73	9.24	8.54	10.2	9.30	9.35	0.83	0.01–0.06
Tb	9.27	8.73	8.70	10.0		9.48	9.74	9.33	8.83	10.1	9.64	9.53	0.65	0.001–0.005
Dy	9.11	8.61	8.88	10.1		9.95	10.0	9.43	8.69	10.3	9.79	9.61	0.84	0.001–0.007
Ho	10.1	9.40	9.18	10.6		10.0	10.0	9.89	9.52	10.6	9.68	9.94	0.59	0.0005–0.002
Er	9.46	8.84	9.23	10.5		10.4	10.3	9.81	9.06	11.0	9.57	9.87	0.99	0.003–0.009
Tm	10.2	9.74	9.50	11.0		10.3	10.6	10.2	9.98	11.0	9.79	10.3	0.68	0.001–0.005
Yb	9.47	8.85	9.18	10.7		10.3	10.0	9.74	9.08	11.0	9.70	9.93	0.99	0.001–0.005
Lu	9.65	8.81	9.19	10.5		9.49	9.67	9.55	9.11	10.6	9.18	9.61	0.82	0.0005–0.003
Hf	4.66	4.66	4.80	4.26		4.26	4.15	4.47	3.98	4.69	4.20	4.29	0.36	0.01–0.04
Pb	64.2	60.5	57.1	72.4		71.5	63.5	64.9	48.3	62.7	57.2	56.0	7.3	0.01–0.03
Th	48.8	43.7	48.5	53.4		52.9	54.2	50.2	44.4	56.1	50.7	50.4	5.9	0.0001–0.0004
U	1.56	1.45	1.34	1.57		1.63	1.28	1.47	1.19	1.58	1.50	1.42	0.21	0.0001–0.0004

LOD (range), range of limits of detection for nanosecond LA measurements, (..), mass fraction uncertain, near LOD.

mass fractions $> 10 \text{ mg kg}^{-1}$) and 30% (at mass fractions of 0.001 mg kg^{-1}). These values are similar to the repeatability of LA-ICP-MS obtained from reference glasses (e.g., NIST, MPI-DING, USGS glasses, Jochum *et al.* 2005, 2006, Jochum *et al.* 2011) and other homogeneous microanalytical samples (e.g., FeMnOx, Jochum *et al.* 2016). The RSD values obtained for the original powder pellets, however, are significantly higher by a factor of about 2–3. This implies that nano-pellets are an important improvement for microanalytical powdered RMs, for example, Ca carbonate samples. In particular, the results for the MACS-3NP are promising, because

MACS-3 is often used as calibration material, and therefore MACS-3NP or nano-pellets of similar Ca carbonate samples are appropriate to replace MACS-3 in the future.

- (2) determination of the repeatability of Mg/Ca. Recently, Jochum *et al.* (2019) have developed a single-shot femtosecond LA-ICP-MS high-resolution technique to determine Mg/Ca in foraminifers using double charged $^{44}\text{Ca}^{2+}$, single charged $^{25}\text{Mg}^{+}$ and MACS-3 for calibration (Figure 2). The ratio of the double charged Ca to the single charged Mg is ca. 1% and independent of the fluence of $0.3\text{--}0.6 \text{ J cm}^{-2}$ (Jochum *et al.* 2019). The newly

Table 2c.

Mass fractions (mg kg^{-1}) and standard deviations (1s) of JcP-1 and JcP-1NP samples using femtosecond (fs) and nanosecond (ns) laser ablation

Spot size	JcP-1					JcP-1NP					Mean JcP-1NP	
	55 μm	55 μm	55 μm	Mean JcP-1		55 μm	25 μm	55 μm	55 μm	25 μm	Mean JcP-1NP	
	fs	ns	ns			fs	fs	ns	ns	ns		
	mg kg^{-1}	mg kg^{-1}	mg kg^{-1}	mg kg^{-1}	1 s	mg kg^{-1}	mg kg^{-1}	mg kg^{-1}	mg kg^{-1}	mg kg^{-1}	mg kg^{-1}	1 s
Li		(0.45)	(0.42)	(0.44)				(0.52)	(0.39)		(0.45)	
B	54.0	49.9	53.2	52.4	2.2	50.6	45.3	46.2	53.8	46.5	48.5	3.6
Na	4260	3650	3800	3900	320	4280	4780	3590	3840	4000	4100	460
Mg	883	876	841	867	23	853	870	864	848	839	855	13
Al	104	79.3	147	110	34	374	399	313	433	378	379	44
Si	388	343	552	428	110	3460	3130	2840	3470	3180	3220	260
P		11.1	15.4	13.3	3.0			14.9	18.9	12.5	15.4	3.2
Ti		1.36	1.79	1.58	0.30			3.94	5.20		4.57	0.89
V	0.195	0.211	0.221	0.209	0.013	0.277		0.245	0.273	0.281	0.269	0.016
Cr		0.533	0.585	0.559	0.037			0.674	0.585		0.629	0.063
Mn		0.746	0.815	0.781	0.049			1.06	1.17	1.15	1.13	0.06
Fe		47.6	55.9	51.8	5.9		64.3	62.1	75.2		67.2	7.0
Co		0.366	0.319	0.342	0.033			0.291	0.339	0.312	0.314	0.024
Ni	0.318	0.629	0.439	0.462	0.157			0.693	0.483		0.588	0.148
Cu		0.673	0.614	0.644	0.042	0.604	1.14	0.696	0.658	0.796	0.780	0.216
Zn		2.0		2.0				2.3	2.0		2.2	0.2
Rb	0.137	0.141	0.201	0.159	0.036	0.589	0.671	0.487	0.587	0.594	0.585	0.065
Sr	6940	6530	6550	6670	230	6910	7390	6700	6520	6930	6890	330
Y	0.246	0.235	0.241	0.241	0.006	0.333	0.337	0.302	0.344	0.333	0.330	0.016
Zr	1.74	1.75	2.40	1.96	0.38	5.28	3.65	5.01	7.47	4.20	5.12	1.47
Cs			(0.01)	(0.01)				(0.017)	(0.023)		(0.020)	
Ba	6.69	6.58	7.65	6.97	0.59	8.99	8.90	8.76	10.0	9.45	9.21	0.49
La	0.0446	0.0550	0.0589	0.0528	0.0074	0.0859	0.0994	0.0833	0.0888	0.0882	0.0891	0.0061
Ce	0.0361	0.0413	0.0598	0.0457	0.0125	0.102	0.100	0.0951	0.112	0.0886	0.100	0.009
Pr	0.00830	0.00954	0.0105	0.00943	0.0011	0.0174		0.0168	0.0195	0.0157	0.0174	0.0016
Nd	0.0372	0.0432	0.0489	0.0431	0.0059	0.0693		0.0680	0.0760		0.0711	0.0043
Sm		0.00781	0.0109	0.00934	0.00215			0.0131	0.0204		0.0168	0.0051
Eu		(0.0011)	0.00299	0.00299					0.00546		0.00546	
Gd		0.0101	0.0165	0.0133	0.0045			0.0198	0.0221		0.0210	0.0016
Tb			0.0023	0.0023				0.0030	0.0044		0.0037	0.0010
Dy		0.0141	0.0134	0.0137	0.0005	0.0181		0.0178	0.0208		0.0189	0.0017
Ho	0.00252	0.00238	0.00364	0.00285	0.00069	0.00458		0.00439	0.00643		0.00513	0.00113
Er		0.00880	0.0135	0.0111	0.0033			0.0136	0.0173		0.0155	0.0026
Tm		(0.00062)	0.00200	0.00200				0.00177	0.00375		0.00276	0.001
Yb			0.0124	0.0124				0.0132	0.0183		0.0158	0.0036
Lu		0.00098	0.00207	0.00152	0.00077			0.00299	0.00390		0.00345	0.00065
Hf	0.0499	0.0512	0.0716	0.0575	0.0122	0.128	0.151	0.144	0.196	0.0907	0.142	0.038
Pb	0.216	0.232	0.260	0.236	0.022	0.292	0.329	0.279	0.297	0.327	0.305	0.022
Th	0.0115	0.00984	0.0174	0.0129	0.0040	0.0393	0.0369	0.0376	0.0499	0.0438	0.0415	0.0054
U	2.67	2.54	2.78	2.67	0.12	2.69	2.57	2.44	2.62	2.86	2.64	0.16

(...), mass fraction uncertain, near LOD.

prepared nano-pellet sample MACS-3NP was also analysed and compared with the Mg/Ca ratios of the original USGS pellet. As Figure 2 shows, the Mg/Ca variation in the fine-grained MACS-3NP sample is significantly more uniform (RSD of six measurements = 0.9%) than that of the original sample (7.1%).

(3) element distribution using 2D mapping following the method by Sfoma and Lugli (2017). Figure 3 shows

a comparison of the element distribution of a 2×2 mm area of the two original pellets and the nano-pellets investigated. The different colours indicate semiquantitative concentration data. Figure 3 therefore only demonstrates the degree of homogeneity. It shows a better microhomogeneity of Sr in MACS-3NP and JcP-1NP as well as of Ba and Rb in MACS-3NP and JcP-1NP, respectively, compared with the original pellets.

Table 2d.
Mass fractions (mg kg^{-1}) and standard deviations (1 s) of JcT-1 and JcT-1NP samples using femtosecond (fs) and nanosecond (ns) laser ablation

Spot size	JcT-1					JcT-1NP					Mean JcT-1NP	
	55 μm (fs)	55 μm (ns)	55 μm (ns)	Mean JcT-1		55 μm (fs)	25 μm (fs)	55 μm (ns)	55 μm (ns)	25 μm (ns)	Mean JcT-1NP	1 s
	mg kg^{-1}	mg kg^{-1}	mg kg^{-1}	mg kg^{-1}	1 s	mg kg^{-1}	mg kg^{-1}	mg kg^{-1}	mg kg^{-1}	mg kg^{-1}		
Li		(0.33)	(0.30)	(0.32)				(0.36)			(0.36)	
B	23.5	22.5	22.7	22.9	0.5	21.7	23.7	22.2	25.2	22.7	23.1	1.4
Na	4510	3910	3980	4130	330	3730	4440	3540	3660	3800	3830	350
Mg	270	287	276	278	9	267	290	290	275	283	281	10
Al	47.5	34.8	62.9	48.4	14.1	192	217	174	224	192	200	20
Si		195	245	220	35	3650	3820	3300	3660	3610	3610	190
P		10.5	13.7	12.1	2.3			11.1	13.1	14.4	12.9	1.7
Ti		(0.6)	(0.8)	(0.7)			5.93	2.16	2.31	4.31	3.68	1.79
V		0.0406	0.0426	0.0416	0.001			0.0692	0.0795		0.0744	0.0073
Cr		0.478	0.457	0.467	0.015			0.453	0.489		0.471	0.026
Mn			(0.5)	(0.5)				0.59	0.49		0.54	0.07
Fe		44.0	48.7	46.4	3.3			56.6	66.4		61.5	7.0
Co		0.0950	0.0897	0.0924	0.0037			0.0835	0.099		0.0910	0.0106
Ni			0.495	0.495				0.585			0.585	
Cu	0.350	0.455	0.444	0.416	0.058	0.796	1.01	0.953	1.05	0.783	0.917	0.122
Zn			(2)	(2)								
Rb		0.0462	0.0777	0.0620	0.022	0.225	0.299	0.217	0.248	0.278	0.253	0.035
Sr	1460	1360	1320	1380	70	1410	1470	1420	1320	1420	1410	50
Y	0.0269	0.0255	0.0243	0.0256	0.0013	0.0590		0.0569	0.0626	0.0604	0.0597	0.0024
Zr	0.768	1.01	1.00	0.925	0.136	4.14	3.15	3.60	4.52		3.85	0.60
Cs	(0.0035)	(0.0031)	(0.0035)	(0.0033)		0.0068		0.0112	0.0098		0.00925	0.00226
Ba	3.42	3.49	4.29	3.73	0.48	5.23	5.23	5.32	6.02	5.71	5.50	0.35
La	0.0116	0.0136	0.0141	0.0131	0.0013	0.0312		0.0296	0.0337	0.0350	0.0324	0.0024
Ce	0.0188	0.0192	0.0235	0.0205	0.0026	0.0494		0.0482	0.0569	0.0621	0.0541	0.0065
Pr		0.00305	0.00293	0.00299	0.00008	0.00699		0.00728	0.00880		0.00769	0.00097
Nd	0.0033	0.0050	0.0125	0.0069	0.0049	0.0246		0.0314	0.0301		0.0287	0.0036
Sm			(0.003)	(0.003)				0.0021	0.0104		0.0063	0.0058
Eu			(0.003)	(0.003)					0.0031		0.0031	
Gd	0.0097		(0.005)	0.0097					0.0104		0.0104	
Tb			(0.002)	(0.002)					0.0025		0.0025	
Dy			0.005	0.005				0.0030	0.0103		0.0067	0.0051
Ho			0.0008	0.0008				0.0013	0.0033		0.0023	0.0014
Er			(0.02)	(0.02)					0.0076		0.0076	
Tm			0.00040	0.00040					0.0015		0.0015	
Yb			0.0024	0.0024				0.0030	0.0090		0.0060	0.0042
Lu			0.0008	0.0008				0.0010	0.0024		0.0017	0.0010
Hf	0.0317	0.0343	0.0332	0.0331	0.0013	0.102		0.0992	0.114		0.105	0.008
Pb	0.0695	0.0750	0.0871	0.0772	0.0090	0.124		0.133	0.130		0.129	0.005
Th	0.00501	0.00476	0.00748	0.00575	0.00151	0.0188		0.0176	0.0221	0.0221	0.0202	0.0023
U	0.0518	0.0639	0.0681	0.0613	0.0085	0.0608	0.0617	0.0598	0.0611	0.0796	0.0646	0.0084

(...), mass fraction uncertain, near LOD.

(4) the three Ca carbonate RMs have high Sr contents ($1400\text{--}7500 \text{ mg kg}^{-1}$; GeoReM database, Jochum *et al.* 2005) and, hence, are suitable RMs for *in situ* Sr isotope analysis (Weber *et al.* 2017). To test possible differences between the data of the original pellets and the nano-pellets, we used LA-MC-ICP-MS to determine $^{87}\text{Sr}/^{86}\text{Sr}$. For these measurements, ten line scans were performed for each RM using the UP213 LA system. Typical duration for a single line was about 3.5 min,

resulting in a total number of about 700 cycles per measurement. Table 4 shows the results of the measurements indicating that the Sr isotope ratios are identical within uncertainty limits for both kind of pellets.

Measurement accuracy

The mass fractions of NIST SRM 612 and NIST SRM 610 used for calibration of the carbonate reference

Table 2e.
Mass fractions (mg kg^{-1}) and standard deviations (1 s) of MACS-1 using femtosecond (fs) and nanosecond (ns) laser ablation

Spot size	55 μm (fs)	55 μm (fs)	55 μm (ns)	55 μm (ns)	25 μm (ns)	Mean MACS-1	
	mg kg^{-1}	mg kg^{-1}	mg kg^{-1}	mg kg^{-1}	mg kg^{-1}	mg kg^{-1}	1 s
Li			(0.4)			(0.4)	
B	18.7	18.6	21.9	22.7	22.1	20.8	2.0
Na	103	95.4	90.2			96.3	6.7
Mg	10.7	12.2	12.8	9.3	13.4	11.7	1.7
Al	21.0	22.3	30.7	23.1	25.5	24.6	3.8
Si			201	(140)	158	180	31
P			14.2	13.7	12.8	13.6	0.7
Ti			(1)			(1)	
V			0.017			0.017	
Cr	103	111	125	116	125	116	9
Mn	115	121	121	112	114	116	4
Fe	148	130	160	163	132	146	16
Co	123	123	118	113	121	120	4
Ni	113	126	127	117	122	121	6
Cu	133	136	120	115	118	124	9
Zn	204	166	119	120	129	148	37
Rb	0.20	0.19	0.20	0.094		0.17	0.05
Sr	241	241	225	214	214	227	13
Y	0.050		0.062	0.048	0.060	0.055	0.007
Zr	0.015		0.026	0.015		0.019	0.006
Cs			(0.01)			(0.01)	
Ba	134	137	119	116	125	126	9
La	116	118	133	121	129	123	7
Ce	108	109	113	107	116	111	4
Pr	0.0061		0.0069	0.0054		0.0061	0.0008
Nd	114	110	132	116	127	120	9
Sm	112	110	128	112	125	117	8
Eu	0.0080		0.0062	0.0048		0.0063	0.0016
Gd	109	107	121	105	119	113	7
Tb	0.027		0.070	0.038	0.028	0.041	0.020
Dy	112	108	131	110	126	117	10
Ho	0.0059		0.0086	0.0060		0.0068	0.0015
Er	109	106	128	108	115	113	9
Tm	0.0048		0.0058	0.0044		0.0050	0.0007
Yb	111	104	123	106	112	111	7
Lu	0.0029		0.0041	0.0025		0.0032	0.0008
Hf			0.023	0.017		0.020	0.004
Pb	139	133	120	109	132	127	12
Th	0.012		0.015	0.012		0.013	0.002
U	0.0031		0.0048	0.0038		0.0039	0.0008

(...), mass fraction uncertain, near LOD.

materials are either certified by NIST or quasi-certified (Jochum *et al.* 2011) using ISO guidelines and have a high level of confidence. Although the NIST glass is not ideal for calibrating carbonate materials, due its silicate matrix and the possible matrix effects this can introduce, we observe only minor effects (< 2%) in the quality of our data when using the nearly matrix-independent fs laser ablation. With the ns-laser ablation, the difference between the data and the 'true' values is less than 5–10% for most refractory elements (Jochum *et al.* 2014).

Overall, the trace element mass fractions in MACS-3NP agree well with those of the original USGS MACS-3 powder pellets with the repeatability of LA-ICP-MS of several per cent. However, there are some significant differences in the element compositions of the nano-pellets and the original pellets (Figure 4). This is especially obvious for the trace element Si, where the content in MACS-3NP and the nano-pellets of GSJ carbonate samples is a factor of 7–16 higher, presumably because of contamination during the nano-pellet preparation using agate milling gear (Garbe-Schönberg and Mueller 2014).

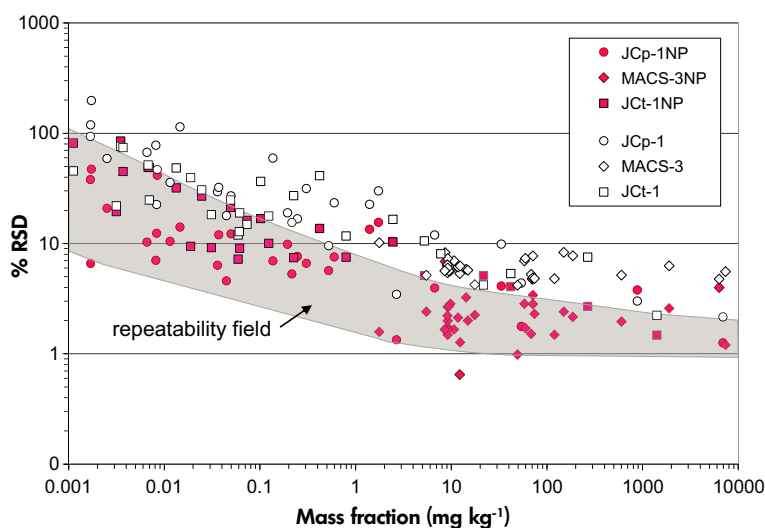


Figure 1. Relative standard deviation (RSD) in per cent vs. mass fraction (mg kg^{-1}). Each data point represents the results of nine line scan trace element measurements using ns-laser ablation (see Table S1). Measurements using nano-pellets (dark symbols) have RSDs that are significantly lower than those obtained from original pellets (open white symbols). Most nano-pellet data points are within the repeatability field of LA-ICP-MS analyses obtained from homogeneous glasses. [Colour figure can be viewed at wileyonlinelibrary.com]

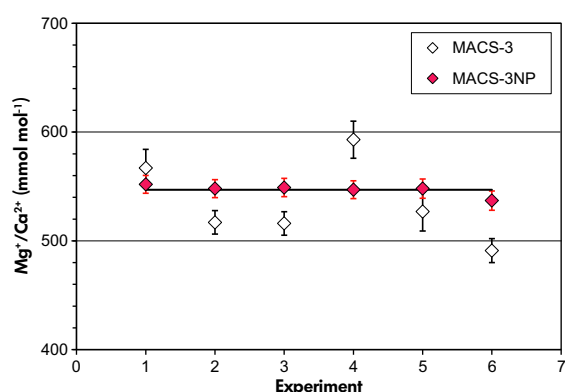


Figure 2. $\text{Mg}^+/\text{Ca}^{2+}$ values of MACS-3 obtained from single-shot analyses (Jochum *et al.* 2019). The variability of six independent measurements is much lower for the nano-pellet sample compared with the original sample. [Colour figure can be viewed at wileyonlinelibrary.com]

Further differences of up to a factor of 4 higher than for the original RMs have been recorded especially for low abundance trace elements in the natural carbonate RMs. Nevertheless, these differences are extremely small and in the ng g^{-1} range for Al, Ba, REE and Zr, Pb, Y, Hf and Th in the trace element poor RMs JCp-1 and JcT-1 where mass fractions of REE are uncertain and close to LODs

(Figure 4). Aliquots of both original powder and processed nano-powder of JCp-1 and JcT-1 were analysed after wet chemistry dissolution, and comparison of the results confirms some contamination with elevated contents of Zr, Hf and Th in a similar range but much less contamination of Al, Rb, Ba and REE in the range of < 1.4 when compared with the original powder (unpublished data DGS). Whether this discrepancy between solution and laser data is related to a matrix effect originating from differential behaviour of nanoparticles during ablation and ionisation in the ICP needs further investigation.

$^{87}\text{Sr}/^{86}\text{Sr}$ data (Table 4) determined by LA-MC-ICP-MS are of high quality and agree well with recently published solution MC-ICP-MS values (Weber *et al.* 2018b). Literature values for the natural RMs JCp-1 and JcT-1 are scarce. For some elements, only one published value or element ratio exist (GeoReM, Hathorne *et al.* 2013), or no data are available at all. Our fs- and ns-LA-ICP-MS data for most elements agree with the literature data when mass fractions are exceeding 1 mg kg^{-1} . However, for some other elements there are large discrepancies. This is the case, for example, for the low abundant REE, where the mass fractions in this work agree with literature data for JcT-1, but are a factor of 10 lower for JCp-1. We believe that this discrepancy possibly results from heterogeneities, analytical effects or bias in the published data.

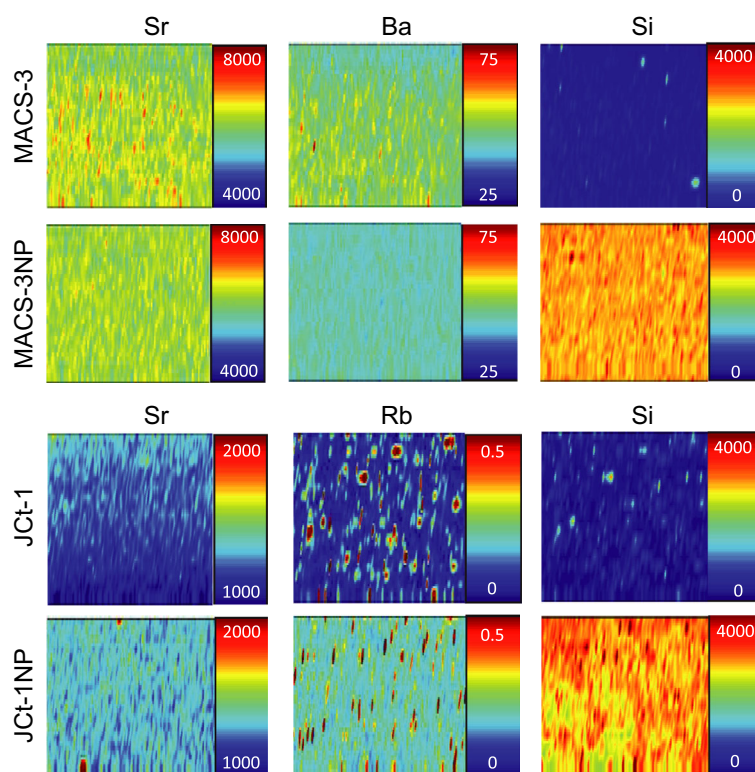


Figure 3. 2D scans (scan direction: bottom to top) of selected elements in MACS-3 and Jct-1 measured in nano- and original pellets, respectively, to demonstrate homogeneity. The different colours indicate only semiquantitative concentration data (mg kg^{-1}) in 2×2 mm areas. [Colour figure can be viewed at wileyonlinelibrary.com]

MACS-3 reference values

The USGS MACS-3 pellets are frequently used for calibrating LA-ICP-MS measurements of Ca carbonate materials. These powder pellets are less homogeneous compared with reference glasses, which are homogeneous in the nanogram to microgram test portion mass range. For the measured MACS-3NP, a homogeneous distribution of most elements similar to that of a glass RM is obtained.

Reliable reference values of MACS-3 pellets and MACS-3NP are important for accurate calibration. Unfortunately, these samples are not certified. Until now, only one compilation data set for MACS-3 pellets from Jochum *et al.* (2012) exists. Table 5 lists our new reference values derived from five data sets: (1, 2) new mass fractions of this paper obtained by fs- and ns-LA-ICP-MS, respectively; (3) reference values compiled in Jochum *et al.* (2012) including data from the USGS; (4) literature values from the GeoReM database (<http://georem.mpch-mainz.gwdg.de/>; Jochum *et al.* 2005); and (5) the average mass fractions obtained from unpublished LA-ICP-MS measurements of JA. Wassenburg between 2015–2017. The

uncertainties of the reference values are mostly between 2% and 7%; exceptions are B, Si, Ti, Zn and the very low abundant Rb and Cs.

As shown earlier (Figure 4), mass fractions of the more homogeneous MACS-3NP agree – except for Si – within uncertainty limits with the original MACS-3 pellets. This means that reference values for MACS-3 pellet may also be used for MACS-3NP. The other two RMs JcP-1NP and Jct-1NP would need re-certification for a number of elements with very low abundance after reworking to nano-powder pellets. However, the majority of elements that are widely used for palaeoclimate studies so far, that is, Na, Mg, Sr, U and Ba, are within uncertainty limits for the natural carbonates.

Conclusions

The analytical data in this paper clearly demonstrate that pellets produced from nano-powdered Ca carbonate RMs are more homogeneous than the original powder pellets by a factor of about 2–3. This finding is improving the quality of microanalytical RMs for LA-ICP-MS, which is important in

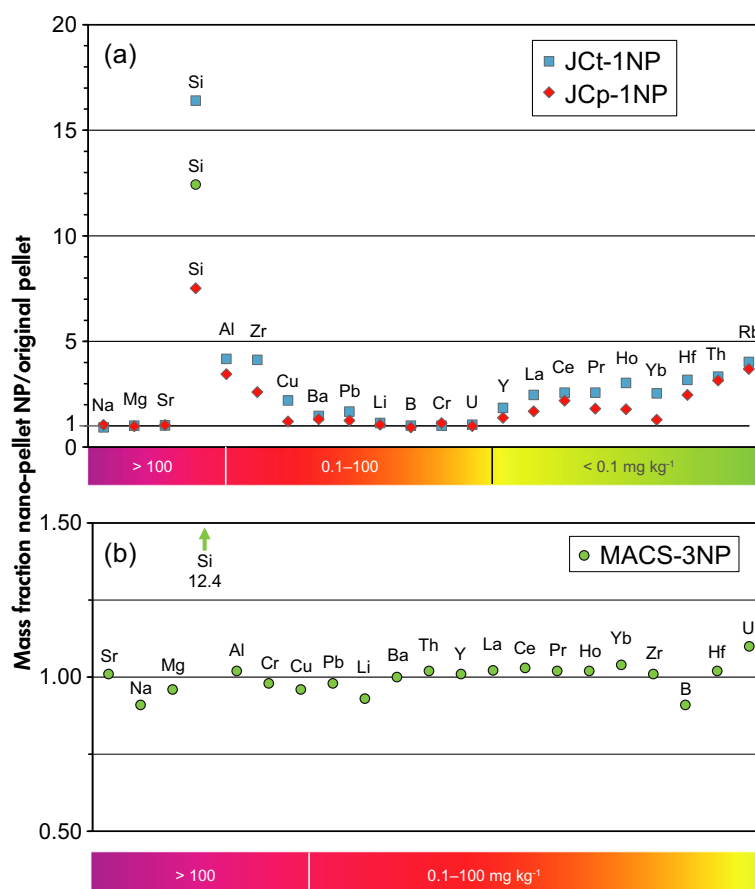


Figure 4. Ratio of mass fractions of nano-pellets and original pellets. (a) Significant differences are found for Si and some low abundant trace elements in Jct-1NP and JCp-1NP. Lithium, B, Na, Mg, Sr, U and other elements are identical within uncertainties in both pellet types. (b) MACS-3NP with high content of all trace elements does not show differences except for Si. [Colour figure can be viewed at wileyonlinelibrary.com]

Table 3.
 $^{87}\text{Sr}/^{86}\text{Sr}$ isotope ratios determined in the original pellets and the nano-pellets (NP) by LA-MC-ICP-MS

Sample	Jct-1	Jct-1NP	MACS-3	MACS-3NP	JCp-1	JCp-1NP
$^{87}\text{Sr}/^{86}\text{Sr}$	0.70917	0.70914	0.70757	0.70755	0.70917	0.70913
2s	0.00005	0.00008	0.00004	0.00008	0.00007	0.00006
$^{84}\text{Sr}/^{86}\text{Sr}$	0.05636	0.05635	0.05603	0.05604	0.05638	0.05636
2s	0.00006	0.00010	0.00006	0.00011	0.00007	0.00009
Weber <i>et al.</i> (2018b)	0.70916		0.70755		0.70916	
95% CL	0.00005		0.00009		0.00005	

They are compared with recently published solution MC-ICP-MS data (Weber *et al.* 2018b).

applications where single-shot analyses at high spatial resolution are utilised. Regrinding of available carbonate RMs leads to contamination of Si and minor proportions of some trace elements and, therefore, indicates the need for re-certification. Because of the urgent need of Ca carbonate

microanalytical RMs in the fast-developing fields of climate geochemistry and environmental research, new RMs should be produced by qualified institutions applying the Garbe-Schönberg and Mueller (2014) method, and certified using ISO guidelines.

Table 4.
Reference values (mass fractions in mg kg⁻¹) for MACS-3

Element	fs This work Mean	ns This work Mean	USGS prel. RV Jochum <i>et al.</i> (2012)	Literature GeoReM Appl.vers. 25 div. labs.	ns This work Wassenburg Mean 2015–2017	RV	1 s
Li	65.8	62.8	62.2	60.7		62.9	2.1
Be			56.4	58.3		57.4	1.3
B	8.07	9.14		6.7	8.80	8.2	1.1
Na	6310	5960	5900	6000	5060	5850	470
Mg	1640	1610	1756	1849	1720	1720	100
Al	370	375		398	439	396	31
Si	(260)	433		363	419	(400)	
P	103	111		94.9		103	8
Cl			61			61	
K				1.1		1.1	
Ca				376900		376900	
Sc			21	19.6		20.3	1.0
Ti	47.6	50.8	54.9	52.1	60.2	53.1	4.7
V	43.6	45.4	46.3	44.0		44.8	1.2
Cr	112	116	117	109		114	4
Mn	513	505	536	531	473	512	25
Fe	9910	10800	11200	10140		10500	600
Co	56.1	55.1	57.1	52.7		55.3	1.9
Ni	56.9	55.6	57.4	54.8		56.2	1.2
Cu	119	113	120	112		116	4
Zn	154	122	111	108		124	21
Ga			16.1	15.0		15.6	0.8
Ge			56.9	54.5		55.7	1.7
As			44.2	48.9		46.6	3.3
Br			0.44			0.44	
Rb	(0.082)	(0.02)		0.039	(0.017)	(0.04)	
Sr	6840	6560	6760	6621	6410	6640	170
Y	22.5	20.0		21.4	19.0	20.7	1.5
Zr	8.38	8.17	8.67	8.62		8.5	0.2
Nb			35.2	50.6		42.9	
Ru			20.1			20.1	
Pd			3.4			3.4	
Ag			53.3	55.6		54.5	1.6
Cd			54.6	52.2	54.8	53.9	1.4
In				0.20		0.20	
Sn			58.1	50.7		54.4	5.2
Sb			20.6	20.0		20.3	0.4
Cs	(0.01)	0.013		0.016		(0.013)	
Ba	59.0	59.3	58.7	58.7	62.1	59.6	1.4
La	10.9	10.4	10.4	10.7	10.6	10.6	0.2
Ce	11.3	10.8	11.2	10.8	10.5	10.9	0.3
Pr	11.7	11.4	12.1	11.3	10.8	11.5	0.5
Nd	11.0	10.3	11.0	10.7	10.0	10.6	0.4
Sm	11.0	10.0	11.0	10.1	9.49	10.3	0.7
Eu	11.4	11.0	11.8	10.8	10.4	11.1	0.5
Gd	10.3	9.24	10.8	9.57	8.69	9.72	0.84
Tb	10.2	9.33		9.67	8.77	9.49	0.60
Dy	10.5	9.43	10.7	10.0	8.89	9.9	0.8
Ho	10.7	9.89	11.3	10.2	9.20	10.3	0.8
Er	11.0	9.81	11.2	10.3	9.17	10.3	0.8
Tm	11.2	10.2		10.6	9.43	10.4	0.7
Yb	11.0	9.74		10.6	9.45	10.2	0.7
Lu	10.6	9.55	10.8	10.1	9.03	10.0	0.7
Hf	4.56	4.47	4.73	4.53		4.57	0.11
Ta			20.5	19.7		20.1	0.6
W			2.16	2.1		2.15	0.01

Table 4 (continued).
Reference values (mass fractions in mg kg⁻¹) for MACS-3

Element	fs This work Mean	ns This work Mean	USGS prel. RV Jochum <i>et al.</i> (2012)	Literature GeoReM Appl.vers. 25 div. labs.	ns This work Wassenburg Mean 2015–2017	RV	1 s
Pt			17.8			17.8	
Au			7.12	7.30		7.21	0.13
Hg			10.2			10.2	
Tl			14.2	16.3		15.3	1.5
Pb	57.7	64.9	56.5	59.4	59.9	59.7	3.2
Bi			19.9	21.3		20.6	1.0
Th	55.2	50.2	55.4	52.9	46.0	51.9	3.9
U	1.29	1.47	1.52	1.37	1.39	1.41	0.09

(–), mass fraction uncertain, only for information.

Availability

If interested in nano-pellet samples please contact DGS (email: dieter.garbe-schoenberg@ifg.uni-kiel.de).

Acknowledgements

We thank the editor and the two reviewers for their helpful comments. Raw data can be obtained from the corresponding author. There are no conflict of interests of author and co-authors.

References

Caragnano A., Basso D., Jacob D.E., Storz D., Rodondi G., Benzoni F. and Dutrieux E. (2014)

The coralline red alga *Lithophyllum kotschyianum* f. *affine* as proxy of climate variability in the Yemen coast, Gulf of Aden (NW Indian Ocean). *Geochimica et Cosmochimica Acta*, 124, 1–17.

Fehrenbacher J.S., Russell A.D., Davis C.V., Gagnon A.C., Spero H.J., Cliff J.B., Zhu Z. and Martin P. (2017)

Link between light-triggered Mg-banding and chamber formation in the planktic foraminifera *Neoglobobulimina dutertrei*. *Nature Communications*, 8, 15441.

Fietzke J. and Frische M. (2016)

Experimental evaluation of elemental behavior during LA-ICP-MS: Influences of plasma conditions and limits of plasma robustness. *Journal of Analytical Atomic Spectrometry*, 31, 234–244.

Garbe-Schönberg D. and Mueller S. (2014)

Nano-particulate pressed powder tablets for LA-ICP-MS. *Journal of Analytical Atomic Spectrometry*, 29, 990–1000.

Hathorne E.C., James R.H. and Lampitt R.S. (2009)

Environmental versus biomineralization controls on the intratest variation in the trace element composition of the planktonic foraminifera *G. inflata* and *G. scitula*. *Paleoceanography*, 24PA4204, <https://doi.org/10.1029/2009PA001742>

Hathorne E.C., Gagnon A., Felis T., Adkins J., Asami R., Boer W., Caillon N., Case D., Cobb K.M., Douville E., deMenocal P., Eisenhauer A., Garbe-Schönberg D., Geibert W., Goldstein S., Hughen K., Inoue M., Kawahata H., Kölling M., Comec F.L., Linsley B.K., McGregor H.V., Montagna P., Nurhati I.S., Quinn T.M., Raddatz J., Rebaubier H., Robinson L., Sadekov A., Sherrell R., Sinclair D., Tudhope A.W., Wei G., Wong H., Wu H.C. and You C.-F. (2013)

Interlaboratory study for coral Sr/Ca and other element/Ca ratio measurements. *Geochemistry, Geophysics, Geosystems*, 14, 3730–3750.

Inoue M., Nohara M., Okai T., Suzuki A. and Kawahata H. (2004)

Concentrations of trace elements in carbonate reference materials coral JCp-1 and giant clam JCt-1 by inductively coupled plasma-mass spectrometry. *Geostandards and Geoanalytical Research*, 28, 411–416.

Jentzen A., Nürnberg D., Hathorne E.C. and Schönfeld J. (2018)

Mg/Ca and $\delta^{18}\text{O}$ in living planktic foraminifera from the Caribbean, Gulf of Mexico and Florida Straits. *Biogeosciences Discussions*, 2018, 1–27.

Jochum K.P. and Enzweiler J. (2014)

Reference materials in geochemical and environmental research. In: Turekian K.K. (ed.), *Treatise on geochemistry* (2nd edition). Elsevier (Oxford), 43–70.



references

Jochum K.P., Willbold M., Raczek I., Stoll B. and Herwig K. (2005)

Chemical characterisation of the USGS reference glasses GSA-1G, GSC-1G, GSD-1G, GSE-1G, BCR-2G, BHVO-2G and BIR-1G using EPMA, ID-TIMS, ID-ICP-MS and LA-ICP-MS. *Geostandards and Geoanalytical Research*, 29, 285–302.

Jochum K.P., Stoll B., Herwig K., Willbold M., Hofmann A.W., Amini M., Aarburg S., Abouchami W., Hellebrand E., Mocek B., Raczek I., Stracke A., Alard O., Bouman C., Becker S., Dücking M., Brätz H., Klemd R., de Bruin D., Canil D., Cornell D., de Hoog C.-J., Dalpé C., Danyushevsky L., Eisenhauer A., Gao Y., Snow J.E., Groschopf N., Günther D., Latkoczy C., Guillong M., Hauri E.H., Höfer H.E., Lahaye Y., Horz K., Jacob D.E., Kasemann S.A., Kent A.J.R., Ludwig T., Zack T., Mason P.R.D., Meixner A., Rosner M., Misawa K., Nash B.P., Pfänder J., Premo W.R., Sun W.D., Tiepolo M., Vannucci R., Vennemann T., Wayne D. and Woodhead J.D. (2006)

MPI-DING reference glasses for *in situ* microanalysis: New reference values for element concentrations and isotope ratios. *Geochemistry, Geophysics, Geosystems*, 7, Q02008.

Jochum K.P., Stoll B., Herwig K. and Willbold M. (2007)
Validation of LA-ICP-MS trace element analysis of geological glasses using a new solid-state 193 nm Nd:YAG laser and matrix-matched calibration. *Journal of Analytical Atomic Spectrometry*, 22, 112–121.

Jochum K.P., Weis U., Stoll B., Kuzmin D., Yang Q., Raczek I., Jacob D.E., Stracke A., Birbaum K., Frick D.A., Günther D. and Enzweiler J. (2011)

Determination of reference values for NIST SRM 610–617 glasses following ISO guidelines. *Geostandards and Geoanalytical Research*, 35, 397–429.

Jochum K.P., Scholz D., Stoll B., Weis U., Wilson S.A., Yang Q., Schwalb A., Bömer N., Jacob D.E. and Andreae M.O. (2012)

Accurate trace element analysis of speleothems and biogenic calcium carbonates by LA-ICP-MS. *Chemical Geology*, 318–319, 31–44.

Jochum K.P., Stoll B., Weis U., Jacob D.E., Mertz-Kraus R. and Andreae M.O. (2014)

Non-matrix-matched calibration for the multi-element analysis of geological and environmental samples using 200 nm femtosecond LA-ICP-MS: A Comparison with nanosecond lasers. *Geostandards and Geoanalytical Research*, 38, 265–292.

Jochum K.P., Wilson S.A., Becker H., Garbe-Schönberg D., Groschopf N., Kadlag Y., Macholdt D.S., Mertz-Kraus R., Otter L.M., Stoll B., Stracke A., Weis U., Haug G.H. and Andreae M.O. (2016)

FeMnOx-1: A new microanalytical reference material for the investigation of Mn–Fe rich geological samples. *Chemical Geology*, 432, 34–40.

Jochum K.P., Jentzen A., Schiebel R., Stoll B., Weis U., Leitner J., Repschläger J., Nürnberg D. and Haug G.H. (2019)

High-resolution Mg/Ca measurements of foraminifer shells using femtosecond LA-ICP-MS for paleoclimate proxy development. *Geochemistry, Geophysics, Geosystems*, 20, 2053–2063.

Leduc G., Garbe-Schönberg D., Regenberg M., Contoux C., Etoumeau J. and Schneider R. (2014)

The late Pliocene Benguela upwelling status revisited by means of multiple temperature proxies. *Geochemistry, Geophysics, Geosystems*, 15, 475–491.

Marali S., Schöne B.R., Mertz-Kraus R., Griffin S.M., Wanamaker A.D., Butler P.G., Holland H.A. and Jochum K.P. (2017)

Reproducibility of trace element time-series (Na/Ca, Mg/Ca, Mn/Ca, Sr/Ca, and Ba/Ca) within and between specimens of the bivalve *Arctica islandica*—A LA-ICP-MS line scan study. *Palaeogeography, Palaeoclimatology, Palaeoecology*, 484, 109–128.

Mertz-Kraus R., Brachert T.C., Jochum K.P., Reuter M. and Stoll B. (2009)

LA-ICP-MS analyses on coral growth increments reveal heavy winter rain in the Eastern Mediterranean at 9 Ma. *Palaeogeography, Palaeoclimatology, Palaeoecology*, 273, 25–40.

Ohata M., Tabersky D., Glaus R., Koch J., Hattendorf B. and Günther D. (2014)

Comparison of 795 nm and 265 nm femtosecond and 193 nm nanosecond laser ablation inductively coupled plasma-mass spectrometry for the quantitative multi-element analysis of glass materials. *Journal of Analytical Atomic Spectrometry*, 29, 1345–1353.

Okai T., Suzuki A., Kawahata H., Terashima S. and Imai N. (2002)

Preparation of a new Geological Survey of Japan geochemical reference material: Coral JCP-1. *Geostandards and Geoanalytical Research*, 26, 95–99.

Schiebel R. and Hemleben C. (2017).

Planktic foraminifers in the modern ocean. Springer-Verlag (Berlin, Heidelberg), 358pp.

Sfoma M.C. and Lugli F. (2017)

MapIT: A simple and user-friendly MATLAB script to elaborate elemental distribution images from LA-ICP-MS data. *Journal of Analytical Atomic Spectrometry*, 32, 1035–1043.

Tabersky D., Luechinger N.A., Rossier M., Reusser E., Hametner K., Aeschlimann B., Frick D.A., Halim S.C., Thompson J., Danyushevsky L. and Günther D. (2014)

Development and characterization of custom-engineered and compacted nanoparticles as calibration materials for quantification using LA-ICP-MS. *Journal of Analytical Atomic Spectrometry*, 29, 955–962.

Vetter L., Spero H.J., Russell A.D. and Fehrenbacher J.S. (2013)

LA-ICP-MS depth profiling perspective on cleaning protocols for elemental analyses in planktic foraminifers. *Geochemistry, Geophysics, Geosystems*, 14, 2916–2931.

Wassenburg J.A., Dietrich S., Fietzke J., Fohlmeister J., Jochum K.P., Scholz D., Richter D.K., Sabaoui A., Spötl C., Lohmann G., Andreae Meinrat O. and Immenhauser A. (2016a)

Reorganization of the North Atlantic Oscillation during early Holocene deglaciation. *Nature Geoscience*, 9, 602–605.

references

Wassenburg J.A., Scholz D., Jochum K.P., Cheng H., Oster J., Immenhauser A., Richter D.K., Häger T., Jamieson R.A., Baldini J.U.L., Hoffmann D. and Breitenbach S.F.M. (2016b)

Determination of aragonite trace element distribution coefficients from speleothem calcite–aragonite transitions. *Geochimica et Cosmochimica Acta*, 190, 347–367.

Weber M., Wassenburg J.A., Jochum K.P., Breitenbach S.F.M., Oster J. and Scholz D. (2017)

Sr-isotope analysis of speleothems by LA-MC-ICP-MS: High temporal resolution and fast data acquisition. *Chemical Geology*, 468, 63–74.

Weber M., Scholz D., Schröder-Ritzrau A., Deininger M., Spötl C., Lugli F., Mertz-Kraus R., Jochum K.P., Fohlmeister J., Stumpf C.F. and Riechelmann D.F.C. (2018a)

Evidence of warm and humid interstadials in central Europe during early MIS 3 revealed by a multi-proxy speleothem record. *Quaternary Science Reviews*, 200, 276–286.

Weber M., Lugli F., Jochum K.P., Cipriani A. and Scholz D. (2018b)

Calcium carbonate and phosphate reference materials for monitoring bulk and microanalytical determination of Sr isotopes. *Geostandards and Geoanalytical Research*, 42, 77–89.

Weber M., Lugli F., Hattendorf B., Scholz D., Mertz-Kraus R., Guinoiseau D. and Jochum K.P. (2019)

NanoSr – A new carbonate microanalytical reference material for *in situ* Sr isotope analysis. *Geostandards and Geoanalytical Research*, in review.

Yang Q., Jochum K.P., Stoll B., Weis U., Bömer N., Schwalb A., Frenzel P., Scholz D., Doberschütz S., Habertzell T., Gleixner G., Mäusbacher R., Zhu L. and Andreae M.O. (2014)

Trace element variability in single ostracod valves as a proxy for hydrochemical change in Nam Co, central Tibet, during the Holocene. *Palaeogeography, Palaeoclimatology, Palaeoecology*, 399, 225–235.

Supporting information

The following supporting information may be found in the online version of this article:

Figure S1. Particle size of Coral JCP-1NP nano-powder as estimated from FE-SEM images.

Table S1. Mass fractions and RSD values obtained from analyses of original and nano-pellet samples of MACS-3, JCP-1 and JCT-1.

This material is available from: <http://onlinelibrary.wiley.com/doi/10.1111/ggr.12292/abstract> (This link will take you to the article abstract).

